

UNCLASSIFIED

AD NUMBER

AD482322

LIMITATION CHANGES

TO:

Approved for public release; distribution is unlimited.

FROM:

Distribution authorized to U.S. Gov't. agencies and their contractors;  
Administrative/Operational Use; 1963. Other requests shall be referred to Naval Postgraduate School, Monterrey, CA.

AUTHORITY

NPS ltr 21 Apr 1972

THIS PAGE IS UNCLASSIFIED

UNCLASSIFIED

AD

482322

DEFENSE DOCUMENTATION CENTER

FOR

SCIENTIFIC AND TECHNICAL INFORMATION

CAMERON STATION, ALEXANDRIA, VIRGINIA



UNCLASSIFIED

NOTICE: When government or other drawings, specifications or other data are used for any purpose other than in connection with a definitely related government procurement operation, the U. S. Government thereby incurs no responsibility, nor any obligation whatsoever; and the fact that the Government may have formulated, furnished, or in any way supplied the said drawings, specifications, or other data is not to be regarded by implication or otherwise as in any manner licensing the holder or any other person or corporation, or conveying any rights or permission to manufacture, use or sell any patented invention that may in any way be related thereto.

**Best  
Available  
Copy**

AD No. 482-322

DDG FILE COPY

UNITED STATES  
NAVAL POSTGRADUATE SCHOOL



THESIS

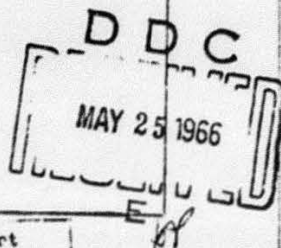
ULTRASONIC MEASUREMENTS IN MANGANESE FLUORIDE IN  
THE REGION OF THE NEEL TEMPERATURE

By

Robert W. Oliver

and

Charles H. Stilwell, Jr.



This document is subject to special export controls and each transmittal to foreign government or foreign nationals may be only with prior approval of the U.S. Naval Postgraduate School (Code 035).

ULTRASONIC MEASUREMENTS IN MANGANESE FLUORIDE IN  
THE REGION OF THE NEEL TEMPERATURE

\* \* \* \*

ROBERT W. OLIVER

and

CHARLES H. STELMER, JR.

6 ULTRASONIC MEASUREMENTS IN MANGANESE FLUORIDE IN  
THE REGION OF THE NÉEL TEMPERATURE

① 1963, 1964,

by

① Robert W. Oliver  
Major, ~~United States Marine Corps~~  
and  
Charles H. Stilwell, Jr.  
Lieutenant, ~~United States Navy~~

Submitted in partial fulfillment of  
the requirements for the degree of

MASTER OF SCIENCE

IN

PHYSICS

United States Naval Postgraduate School  
Monterey, California

① 1963,

① 29p.

ULTRASONIC MEASUREMENTS IN MANGANESE FLUORIDE IN  
THE REGION OF THE NÉEL TEMPERATURE

by

Robert W. Oliver

and

Charles H. Stilwell, Jr.

This work is accepted as fulfilling  
the thesis requirements for the degree of

MASTER OF SCIENCE

IN

PHYSICS

from the

United States Naval Postgraduate School

*John B. Neigham*  
Faculty Advisor

*W. P. Anderson*  
Chairman  
Department of Physics

Approved:

*A. E. C. V. L. L.*  
Academic Dean

#### ACKNOWLEDGMENT

The authors wish to express their appreciation for the enthusiastic guidance of Professor John R. Neighbours and the assistance of Lieutenant Commander Frank H. Featherston, U.S.N., and Mr. Lynwood F. May of the U. S. Naval Postgraduate School.

#### ABSTRACT

↓  
Ultrasonic wave velocities were measured in  $\text{MnF}_2$  in the region of the antiferromagnetic transition. Both longitudinal and shear waves were propagated in the  $[110]$  direction at frequencies up to 65 mc. The longitudinal waves showed an attenuation peak at the  $N_{50}$  temperature which increased with frequency. A magnetic field of 7.6 kilogauss narrowed the attenuation peak slightly, but had no effect on the amount of attenuation, the location of the peak, nor on the velocity. Shear waves exhibited a gradual increase in attenuation with decreasing temperature, but had no attenuation peak. A magnetic field of 5.5 kilogauss increased the attenuation of the shear waves very slightly. Although it was not possible to determine a complete set of moduli, the values at 70° K. appropriate to the waves measured are, in units of  $10^{11}$  dyne  $\text{cm}^{-2}$ :

$$2C_{11} + 3C_{12} + C_{66} = 16.02$$

$$C_{44} = 3.357$$

$$\frac{1}{2}(C_{11} - C_{12}) = 1.727$$

# TABLE OF CONTENTS

	Page
Introduction	1
Experimental Procedure	2
Experimental Results	14
Discussion of Results	23
Appendix I (Calculations)	28

# LIST OF ILLUSTRATIONS

Figure		Page
1.	Sample preparation holder and crystal orientation	3
2.	Sample holder	5
3.	Schematic diagram of experimental apparatus	7
4.	Typical shear wave echoes with superimposed exponential wave	10
5.	Attenuation versus temperature for longitudinal waves in $MnF_2$	16
6.	Attenuation versus temperature for longitudinal waves in $MnF_2$ with applied magnetic field	19
7.	Attenuation versus temperature for shear waves in $MnF_2$	21
8.	Attenuation versus temperature for shear waves in $MnF_2$ with applied magnetic field	22

# LIST OF TABLES

Table		Page
I	Velocities and corresponding moduli for elastic waves propagated in $[110]$ direction in $MnF_2$ .	15
II	Relative change in attenuation at Néel temperature for longitudinal waves propagated in $[110]$ direction in $MnF_2$ .	18
III	Wave length of elastic waves propagated in $[110]$ direction in $MnF_2$ .	27

# INTRODUCTION

The concept of antiferromagnetism was first advanced by Néel in 1932 in connection with his studies of the susceptibility of transition metals and alloys. He noticed that Pt, Pd, Mn Cr, and many of their alloys show an anomalously large temperature independent paramagnetic susceptibility. Néel assumed that the arrangement of atomic moments in a crystal lattice is such that they are antiparallel at a sufficiently low temperature. Using this model he showed that an antiferromagnet obeys the Curie-Weiss law at high temperatures, and was able to obtain formulas for the antiferromagnetic Curie or Néel point.

Since these early investigations many substances other than the transition metals have been investigated. Manganese fluoride is one of these. At its Néel temperature ( $\sim 67^\circ K.$ ) anomalies appear in the magnetic susceptibility, the specific heat, the thermal expansion, neutron scattering and nuclear magnetic resonance frequency. The mechanical properties near the Néel temperature had not been determined, and thus the present work was undertaken.

# EXPERIMENTAL PROCEDURE

A large randomly oriented single crystal of  $MnF_2$  was purchased from the Optovac Corporation. One of the faces of the unoriented rough sample was smoothed by use of 3/0 emery finishing paper on a smooth planar glass surface. A back reflection Laue pattern of this face showed it to be perpendicular to the  $[110]$  direction of the crystal. To obtain another flat face parallel to the first, the sample was placed in a sample preparation holder as shown in Fig. 1. The smoothed face was placed face down inside of the annular region of the holder which was resting on a smooth planar glass surface. This preparation holder was constructed of machined aluminum with the upper and lower faces parallel to within 0.001 inches. With the sample in position in the annular region of the holder, molten sealing wax was poured into the empty regions, forming a rigid bond between the sample and the holder. When the wax had solidified the glass surface was removed, leaving the bottom face of the sample co-planar with the holder. The upper face was then finished with 3/0 emery finishing paper, taking care not to disturb the co-planar aluminum holder surface. When the upper sample face was co-planar with the holder it was considered to be co-planar with the lower face. The sample was then removed by heating the sealing wax.

The upper face, lower face and two of the rough side faces of the sample were then coated with Dow Corning Silicone Fluid No. 710. These four faces of the sample then were wrapped with a single thickness of 0.001 cm aluminum coated mylar film which served as a radio frequency ground for the transducer. The silicone

Coplanar Holder

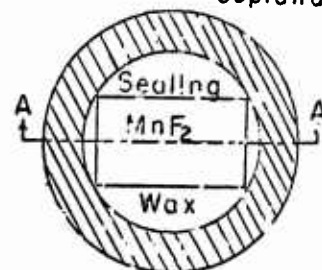
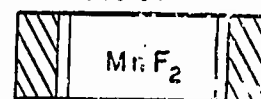


Fig. 1a Sample Preparation Holder



View A-A

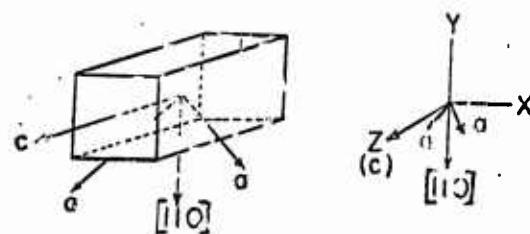


Fig. 1b Orientation of  $MnF_2$

fluid was then applied to the upper surface of the mylar, and a quartz transducer was placed on this fluid. Bonding with substances other than Dow Corning 710 was attempted, but the bonds were either too fragile, or the bonding material caused too great of an inherent bonding attenuation. The sample was then mounted in the sample holder.

Fig. 2 shows the sample holder. Plates A and D of the sample holder are fixed in position and made rigid by three brass machine screws (not shown in Fig. 2). Plate B is constructed of fiber-board, and is used to guide the various wires used in the holder. Plate C is a brass plate that slides vertically on the three brass machine screws, and is fixed in position by positioning nuts on the three screws on both sides of the plate. Mounted in the center of plate C is a dielectric centerpiece with the center lead of the coaxial cable mounted on a brass rod that slides through the dielectric. The end of this rod is then mounted to a circular copper piece that is held in position against the quartz transducer by a coil spring between it and the dielectric. The sample is placed between plates C and D, and plate C is then lowered and secured in a position such that the copper r-f piece is firmly against the quartz transducer. The mylar film touches plate D, forming the electrical contact for the r-f ground return, the holder itself being electrically grounded.

After placing the sample in the sample holder, the entire holder head assembly is pre-cooled and then immersed in the cryogenic fluid. The Dow Corning 710 provides a stable, secure bond of the transducer to the mylar, and of the mylar to the sample. The

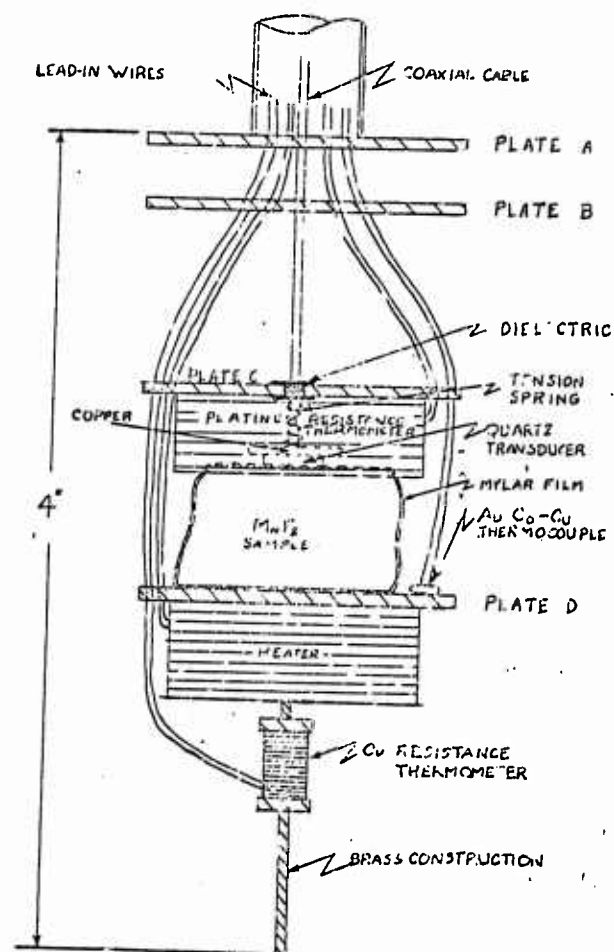


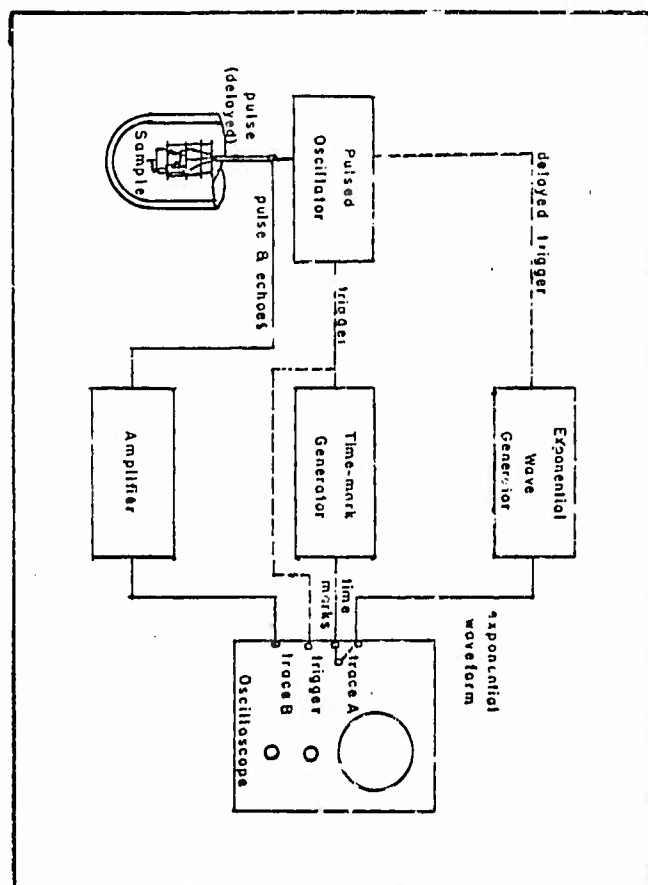
FIG. 2 SAMPLE HOLDER

spring pressure against the copper r-f piece insures contact between the copper and the quartz transducer.

The initial radio frequency wave is generated by an Arenberg Pulsed Oscillator using various frequencies from 5 to 70 mc, and a pulse length of approximately two microseconds. The wave is fed simultaneously to the sample holder, and, through the amplification stages, to a Tektronix RM 45A Oscilloscope. Radio frequency waves excite sound waves in the piezoelectric quartz transducer, and these waves are transmitted through the sample. Echoes return to the quartz transducer where they excite radio frequencies in the quartz, which are then amplified and displayed on the oscilloscope in the proper time relation to the original pulse. The oscillator is externally triggered to pulse at 1000 pulses per second, allowing ample time for the measurement of the returning echoes.

A schematic diagram of the electronic apparatus used in this experiment is shown in Fig. 3. The pulsed oscillator is triggered by a time mark generator which also generates accurate timing marks for display on the oscilloscope. The time-mark trigger also synchronizes the oscilloscope to make both traces begin at the same time the pulsed oscillator is triggered. The pulsed oscillator has a built-in trigger delay to allow accurate reading of the initial pulse. The exponential wave generator is triggered with the same delayed trigger to insure the exponential wave starts the same time the sample is pulsed. The pulse is fed to the sample and through the amplifier simultaneously, and displayed on trace B of the oscilloscope. Returning echoes appear in time phase after amplification on trace B. In velocity measurements, time marks are

Fig. 3 Schematic diagram of experimental apparatus.



placed on trace A which allows an accurate method for the determination of the time between pulses. When attenuation is measured the generated exponential wave is displayed on trace A, and fitted to the envelope of the echo pattern by superimposing trace A on trace B.

Velocity of the wave is determined by measuring the time required for the pulse to transit the sample, reflect from the opposing face, and re-transit the sample, and by measuring the distance traveled (corrected for thermal expansion of the sample).

Transit time is the time required for the pulse to make this round trip. The transit time is measured by determining the time from a given pulse to a series of following pulses, with the aid of a time-mark generator. The time is then plotted as a function of echo number, and an average transit time for a given temperature is obtained from the

The room temperature sample length was determined by a series of micrometer measurements to be  $1.386 \pm 0.001$  cm. The thermal expansion coefficients for  $\text{MnF}_2$  were examined<sup>1</sup>, and found to have negligible effect on the measured length to within the accuracy of the transit time measurements in the temperature region being investigated. Accordingly expansion of the sample was ignored, and the velocity of propagation was obtained by dividing the mean path length by the average transit time. Time was determined to within 0.01 microsec. for transit times of over four microsec. The absolute accuracy of the velocity was determined to 0.2%, although measurements of the

relative change in velocity through the Néel temperature were accurate to 0.01%.

Attenuation was measured originally by measuring the amplitude of successive pulses, and plotting the results against echo number on semi-logarithm paper. The resulting plot was a straight line whose slope was a measure of attenuation per unit time. These measurements were converted into  $\text{db cm}^{-1}$  through the velocity.

In later experiment, an exponential wave was generated and calibrated by use of resistance-capacitance circuits, and used for comparison with the envelope formed by the echoes. Fig. 4(a) shows echoes typical of the shear waves. The time scale is 10 microsec. per cm. Examining the envelope of the echoes evidences the exponential decay. Fig. 4(b) shows the exponential wave generated by the exponential wave generator as is displayed on trace of the oscilloscope. Fig. 4(c) shows the two traces superimposed. The exponential wave fitted to the echo pattern envelope. The two patterns were matched by varying the gains of the amplifier, oscilloscope, and the exponential wave generator, and by varying the time constant of the exponential wave generator by means of a graduated variable resistor.

The exponential wave generator was calibrated by placing a specified setting on the variable resistor of the generator, and recording ten amplitudes at equal time intervals. This data was plotted as a function of the setting of the variable resistance on the exponential wave generator. This calibrated the generator so that in subsequent experimental runs it was necessary to read only the setting of the resistance dials to determine the attenuation as a function of time. This attenuation is directly convertible to

<sup>1</sup>D. F. Gibbons, Phys Rev 115 1194 (1959)

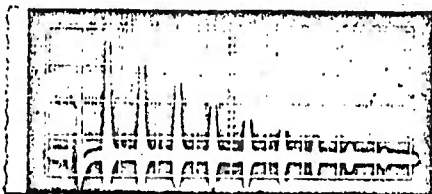


Fig. 4a Shear wave echoes in  $\text{MnF}_2$



Fig. 4b Exponential wave

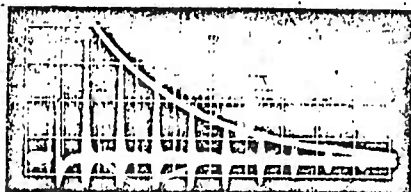


Fig. 4c Exponential wave matched to shear wave echo pattern.

attenuation as a function of distance. The dial could be read to four significant figures, which gives an accuracy of  $\pm 0.001 \text{ db cm}^{-1}$  in attenuation below  $1.5 \text{ db cm}^{-1}$ , and an accuracy of  $\pm 0.002 \text{ db cm}^{-1}$  in the region from  $1.5$  to  $2.4 \text{ db cm}^{-1}$ . Above  $2.4 \text{ db cm}^{-1}$  the accuracy in attenuation measurements decreases rapidly due to limitations in determination of the slope of the exponential wave generated by the exponential wave generator. The maximum attenuation point was readily discernable, but the actual attenuation may be as much as one  $\text{db cm}^{-1}$  more than that indicated by measurement. This possible inaccuracy affects the maximum attenuation measurement of only the  $65.5 \text{ mc}$  frequency. Removal of the trace of the exponential wave, and then replacing and refitting it to the envelope, was within five digits in the fourth significant figure. If the exponential wave trace were fitted continuously to the echo pattern reproducibility was to within one digit in four significant figures.

Initial temperature measurements were made with a copper resistance thermometer placed in a position as indicated in Fig. 2. Experiments were performed using liquid oxygen as a cryogenic, and calibrating the resistance thermometer against equilibrium vapor pressure readings<sup>2</sup>. Comparisons indicated a requirement for a more accurate and reproducible electrical measurement. A gold-cobalt vs copper thermocouple was employed at a position closer to the sample, as shown in Fig. 2, but its accuracy was limited to approximately  $\pm 0.15$  degrees in the temperature range under investigation. Finally a sample of very high purity platinum wire was purchased from the

<sup>2</sup> H. J. Hoge, Journ. Res. NBS 44 321 (1950)

Western Gold Corporation; was varnished, wound, and placed in the position shown in Fig. 2 to more accurately determine the temperature. Resistance was measured accurately to within three milliohms which gives an accuracy in temperature of  $\pm 5$  millidegrees based upon published data<sup>3</sup>. In addition to more accurate temperature determinations, it was found that the time required for the platinum wire resistance thermometer to reach thermal equilibrium was almost exactly that required for the  $\text{MnF}_2$  sample to reach thermal equilibrium. When shifting to a new temperature by varying the pressure on the cryogenic bath the vapor pressure would reach a steady condition initially, followed in a few seconds by the copper resistance thermometer reaching steady state, and this followed almost immediately by the gold-cobalt vs copper thermocouple. Finally from ten to thirty seconds later, depending upon the amount of temperature shift, the platinum resistance thermometer would reach equilibrium. Measurements made on the sample after the platinum resistance thermometer had reached equilibrium were completely reproducible, whereas measurements made prior to this equilibrium might indicate an inaccurate temperature, the error being dependent upon the amount of temperature shift and whether the sample was being cooled or warmed.

Liquid oxygen was chosen as the cryogenic fluid because of its stability and temperature range under readily obtainable pressures in the temperature region under investigation. It is noted that the liquid oxygen has a high heat capacity, and that accurate vapor pressure measurements may be obtained only if the oxygen is kept

boiling at a constant rate. Glass dewar systems were employed to insure that the boiling was occurring while the vapor pressure measurements were made. Glass beads were placed in the bottom of the dewar to act as nuclei for vapor bubbles to form at the bottom of the fluid bath, resulting in continuous boiling, thereby contributing to a more uniform temperature throughout the cryogenic. In making measurements with a magnetic field a metal dewar with a smaller diameter than the glass dewar was used in order to have the maximum possible magnetic field on the sample. Since the boiling could not be observed with a metal dewar, the prime method of temperature determination was by electrical means.

<sup>3</sup> H. J. Hoge & F. G. Brickwedde, Journ. Res. NBS 22 351 (1939)

# EXPERIMENTAL RESULTS

Velocity and attenuation measurements in  $\text{MnF}_2$  were made both with a magnetic field and without a magnetic field in the temperature range from 56 to 80 degrees Kelvin, for both longitudinal and shear waves, using frequencies in the 8.3 to 65.5 mc range.

The velocity of sound of the longitudinal wave in the  $\text{MnF}_2$  sample was constant with temperature and frequency within the region measured to within the accuracies of measurement. The velocity of the longitudinal wave was determined to be  $6.60 \times 10^5$  cm sec<sup>-1</sup>. The velocity of the shear wave was dependent upon the polarization, but independent of frequency and temperature in the region considered. When the wave was excited parallel to the c axis the velocity was determined to be  $2.94 \times 10^5$  cm sec<sup>-1</sup>. Perpendicular excitation waves had a velocity of  $1.62 \times 10^5$  cm sec<sup>-1</sup>. These results are summarized in Table I along with the combination of elastic constants determined from the velocity measurements. The density used in computing the elastic constants was taken to be  $3.891$  gm cm<sup>-3</sup> as listed in the ASTM card file<sup>4</sup>.

The attenuation of longitudinal and shear waves in  $\text{MnF}_2$  was dependent on temperature and frequency. For longitudinal waves there was a large increase in attenuation in the vicinity of the Néel temperature, 67.336 degrees Kelvin<sup>4</sup>. This peak is shown in Fig. 5 where attenuation is plotted as a function of temperature for several different sound frequencies. The peak attenuation was

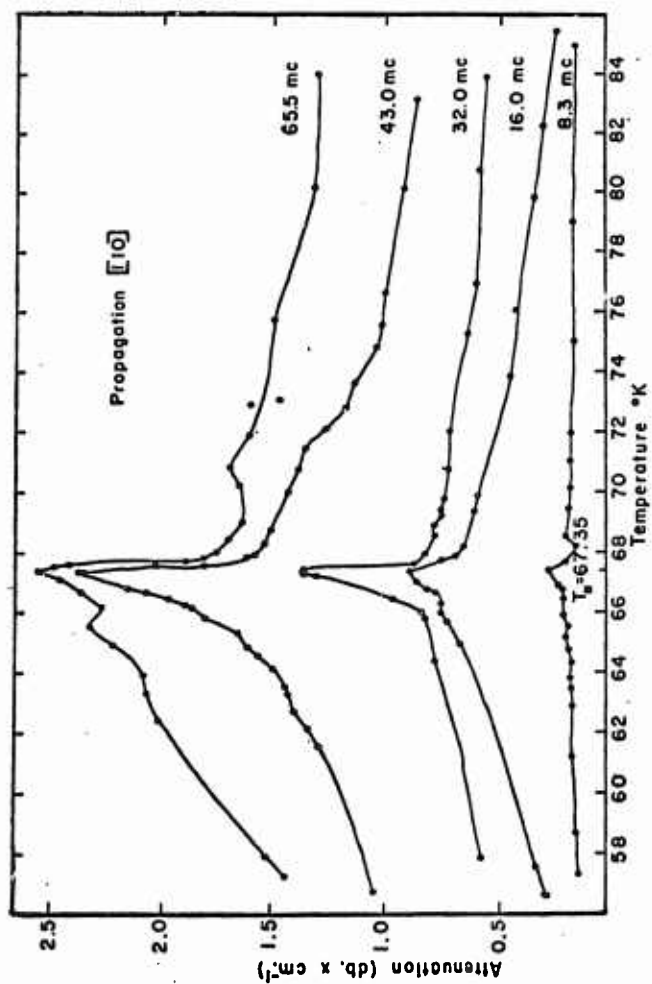
TABLE I

Measured velocities and corresponding moduli for propagation of elastic waves in the  $[110]$  direction in  $\text{MnF}_2$  near the Néel temperature.

Polarization	Velocity (cm sec <sup>-1</sup> )	Modulus (dyne cm <sup>-2</sup> )
$[110]$	$6.60 \times 10^5$	$\frac{1}{2}C_{11} + \frac{1}{2}C_{12} + C_{66} = 16.92 \times 10^{11}$
$[001]$	$2.94 \times 10^5$	$C_{44} = 3.57 \times 10^{11}$
$[1\bar{1}0]$	$1.62 \times 10^5$	$\frac{1}{2}(C_{11} - C_{12}) = 1.19 \times 10^{11}$

<sup>4</sup> P. Heller and G. B. Benedek, Phys. Rev. Letters **8** 428 (1962)

Figure 5  
Attenuation vs temperature for longitudinal waves in  $\text{MnF}_2$ .



centered at the Néel temperature, which, by this present experiment was determined to be  $67.35 \pm .02$  degrees Kelvin. The peak increased in magnitude and became relatively sharper with increasing sound frequency. Except for the lowest frequency (8.3 mc) the attenuation increased with decreasing temperature, rising significantly several degrees in anticipation of the Néel temperature. Within the limits of accuracy of temperature measurements the peak attenuation did not shift position with increasing frequency. The results of the change in attenuation for various frequencies is summarized in Table II.

The effect of an applied magnetic field on the attenuation of longitudinal waves near the Néel temperature is shown in Fig. 6. This figure shows attenuation for 25 mc longitudinal waves plotted in an expanded temperature scale. The filled circles show the attenuation for zero applied field and are in agreement with Fig. 5. The open circle points show the attenuation for a 3.6 kilogauss magnetic field oriented parallel to  $[110]$  and the crosses show attenuation for the same field oriented parallel to  $[001]$ . It is apparent that the magnetic field did not affect the magnitude or the position of the attenuation peak. However, the amount of attenuation immediately adjacent to the Néel temperature was decreased slightly with an applied magnetic field, causing an apparent narrowing of the attenuation peak.

Attenuation of shear waves in  $\text{MnF}_2$  was measured at three frequencies, 10, 15 and 30 mc, for oscillations parallel to the c axis, and at one frequency, 15 mc, for oscillations perpendicular to the c axis. Fig. 7 shows that, for zero magnetic field, attenuation was

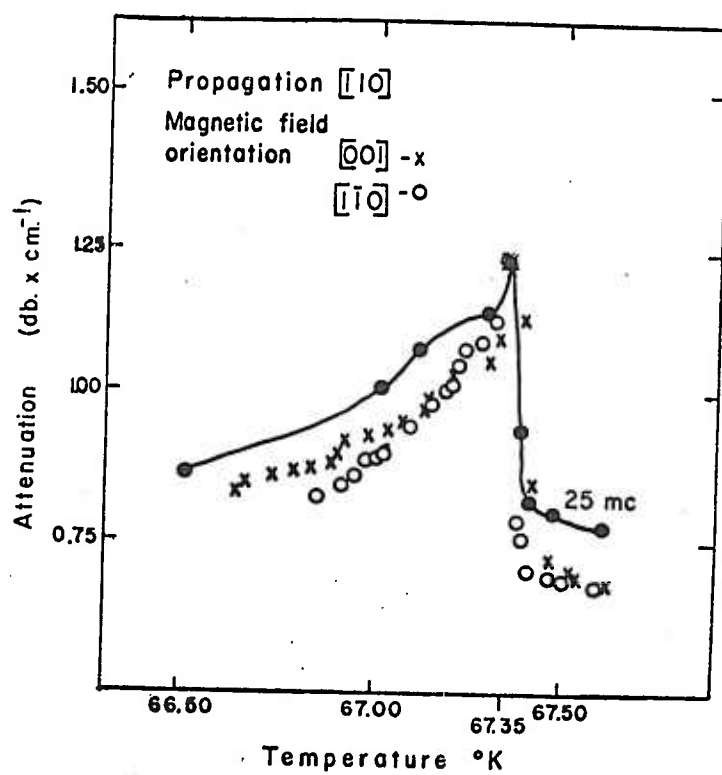
TABLE II

Relative changes in attenuation of longitudinal waves propagating in the  $[110]$  direction in  $\text{MnF}_2$  at the Néel temperature.

Frequency (megacycles sec <sup>-1</sup> )	Attenuation (db cm <sup>-1</sup> )
8.3	0.1
16.0	0.6
32.0	0.8
43.0	1.6
65.5	1.1

Figure 6

Attenuation vs temperature for longitudinal waves in  $\text{MnF}_2$  with 3.6 kilogauss magnetic field applied. (Solid curve is for zero applied field).



found to be dependent on frequency and polarization of the oscillations with only slight dependence on temperature. For the 15 mc waves the attenuation was approximately tripled for a change in polarization oscillation from parallel to the c axis to perpendicular to the c axis, although part of this effect may have been due to differences in bonding. With the polarization parallel to the c axis, the actual attenuation varied as a function of frequency, but the change in the attenuation was approximately constant, and not a function of frequency. It was noted that for 15 mc shear waves there was a slight decrease in attenuation near the Néel temperature for both polarizations. This decrease did not appear with either the 10 mc or 30 mc waves that were measured.

Attenuation of shear waves with polarization parallel to the c axis was measured at 10 mc for a magnetic field of 5.5 kilogauss oriented both parallel and perpendicular to the c axis as shown in Fig. 8. The attenuation was found to be slightly dependent upon the orientation of the magnetic field, with the higher attenuation occurring with the field perpendicular to the c axis. The temperature dependence of the attenuation of the shear waves in the magnetic field was small, and was of the same characteristic as the attenuation without a magnetic field.

Figure 7

Attenuation vs temperature for shear waves in  $\text{MnF}_2$ .

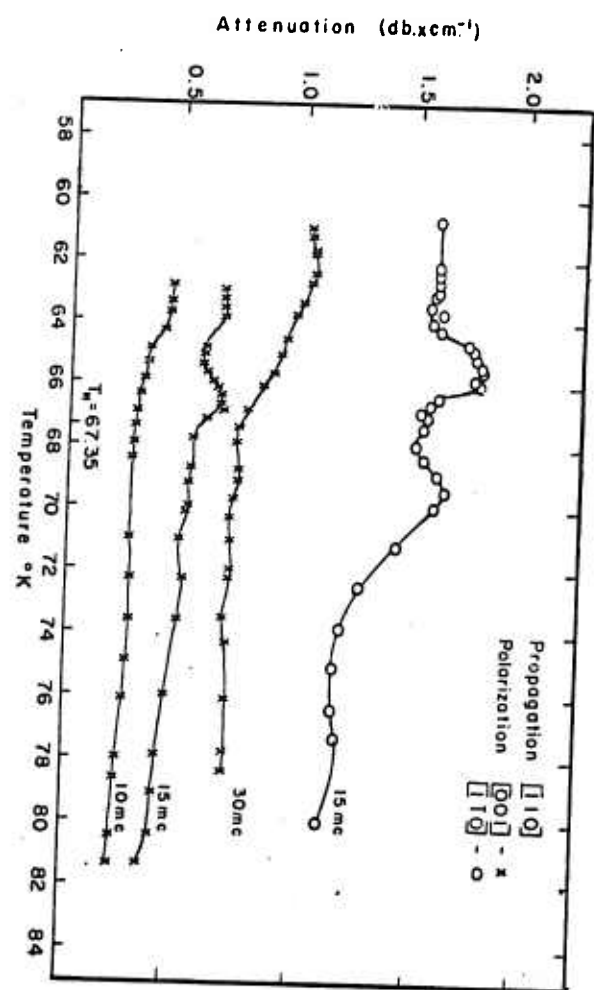
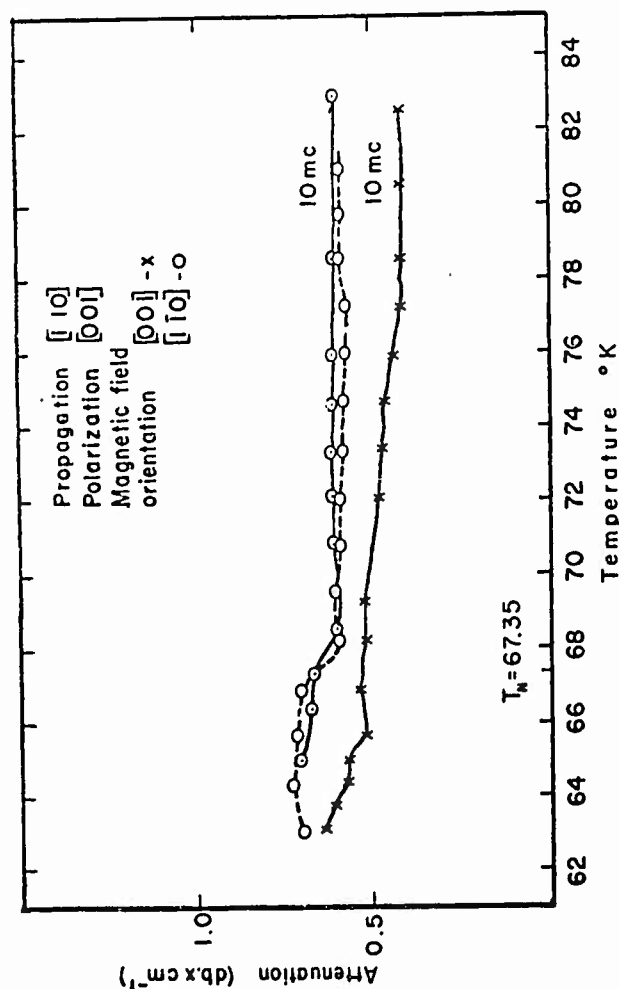


Figure 8  
Attenuation vs temperature for shear waves in  $MnF_2$  with 5.5 kilogauss magnetic field applied. (Data points enclosed in circles indicate run made while warming; open circle points indicate run made while cooling)



#### DISCUSSION OF RESULTS

Changes in many physical properties including internal friction and Young's modulus have been measured near the Néel temperature for other antiferromagnetic materials. The mechanical properties of the metal chromium have been extensively investigated,<sup>5-10</sup> and show anomalies at temperatures of 120° K. and 310° K. Recent low frequency measurements at 1 cycle<sup>8</sup> and at 35 kc<sup>9</sup> show that the changes in mechanical properties are characterized by a dip in Young's modulus and a rise in internal friction at the Néel temperature (310° K.). Both effects persist down to the spin flip temperature ( $\sim 120^\circ$  K.) so that the resultant curves for well annealed samples as functions of temperature show a "channeled" lowering of modulus and an enhancement of attenuation between the two temperatures. The maximum value of attenuation appears near the "spin flip" temperature. These results are in agreement with Overhauser's treatment<sup>10</sup> of the antiferromagnetism of chromium as spin density waves rather than localized moments. The relatively small heat capacity anomaly<sup>6</sup> of chromium near the Néel temperature is also explainable in these terms.

Other results<sup>5</sup> obtained at higher frequency (70 kc) show dips in the modulus and a peak in the internal friction centered at the Néel temperature. Detailed 10 mc measurements<sup>11</sup> of the elastic constants of chromium show that curves of the individual constants as functions of

- <sup>5</sup>M. E. Fine, E. S. Geiner and W. C. Ellis, *J Metals* **189** 56 (1951)
- <sup>6</sup>R. H. Beament, H. Chihara and J. A. Morrison, *Phil Mag* **2** 188 (1960)
- <sup>7</sup>M. deMorton, *Phil Mag* **6** 825 (1961)
- <sup>8</sup>M. deMorton, *Phys Rev Letters* **10** 208 (1963)
- <sup>9</sup>A. Street, *Phys Rev Letters* **10** 210 (1963)
- <sup>10</sup>A. W. Overhauser, *Phys Rev* **128** 1437 (1962)
- <sup>11</sup>D. I. Bolef and J. Deklerk, *Phys Rev* **129** 1063 (1963)

temperature resemble the lower frequency results<sup>9</sup> on unannealed specimens. Dips in the moduli are evident at both the spin flip and Néel temperatures but the internal friction was not determined.

Experiments on oxides of cobalt,<sup>12, 13</sup> nickel,<sup>13</sup> and manganese<sup>14</sup> show similar effects: a lowering of modulus and an increase in internal friction as the temperature is lowered past the Néel temperature. For MnO and CoO changes in modulus and well-developed peaks in internal friction are observed and found to occur at temperatures somewhat below the Néel temperatures. A thermodynamic treatment<sup>14</sup> predicts that the internal friction peak and the change in modulus always occur together and that the maximum in the internal friction always occurs at a temperature lower than the Néel temperature.

Anomalous behavior of ultrasonic attenuation also has been observed<sup>15, 16</sup> in the ferrite  $\text{Fe}_2\text{O}_3$  (magnetite). In magnetite, the internal friction of torsion oscillations of a [100] rod show a peak some 20° K. below the transition temperature while the internal friction of longitudinal oscillations shows no such peak. This material changes structure upon ordering and the anomalous attenuation and modulus change have been interpreted as due to a stress induced ordering. The change in the degree of order caused by a constant applied stress is a maximum at the transformation temperature.

The present results differ from the results quoted above and are

<sup>9</sup> Street, Phys Rev Letters 10 210 (1963)

<sup>12</sup> M. E. Fine, Rev Mod Phys 25 158 (1953)

<sup>13</sup> R. Street and B. Lewis, Nature 168 1036 (1951)

<sup>14</sup> K. P. Belov, G. I. Katayev and R. Z. Levitin, Journ Appl Phys 31 1533 (1960)

<sup>15</sup> M. E. Fine and M. T. Kenney, Phys Rev 94 1573 (1954)

<sup>16</sup> D. F. Gibbons, Journ Appl Phys 28 810 (1957)

characterized by:

- no change in wave velocity was observed at the Néel temperature.
- an attenuation peak for longitudinal waves at the Néel temperature which increases with frequency.
- no observed change in this peak as a result of applied magnetic field.
- an absence of an attenuation peak at the Néel temperature for the shear waves.
- a slight dependence of shear wave attenuation on the orientation of applied magnetic field.

No change in acoustic wave velocity was observed for each of the three polarizations when the sample temperature was lowered through the Néel temperature. Any velocity change is estimated to be less than one part in 5000 and a change in modulus is apparent only through the thermal expansion. For  $\text{MnF}_2$  the change in length along the *a* axes first decreases and then increases with decreasing temperature; being zero at 80° K. Thus the change in modulus through the Néel temperature is seen only through the change in thermal expansion parallel to the *c* axis. For a temperature change from 70° K. to 60° K. this change amounts to about three parts in 10<sup>4</sup>.

The attenuation peak for the longitudinal waves occurred at 67.35° K. for all frequencies measured. The maximum value observed was over 2.6 db  $\text{cm}^{-1}$ . Although the peak is approximately of the same magnitude as that observed for MnO and CoO, no large accompanying change in modulus is observed. (The modulus changes observed in MnO and CoO at lower frequencies were approximately fifty percent.) No thermal hysteresis was evident in

the longitudinal wave experiments although an apparent small thermal hysteresis for shear waves is shown in Fig. 8. In this figure the open circle points show the attenuation of shear waves while cooling and the dotted center points are for warming. These points are close enough together to be within the absolute experimental error.

As shown in Fig. 6, the effect of an external magnetic field is to slightly diminish the attenuation in the vicinity of the maximum, but not to affect the magnitude or position of the maximum. In view of the large internal field in  $\text{MnF}_2$  it is probable that any change in peak height or position will become observable only with the application of much larger fields than the present experiment allows.

For shear waves, an attenuation peak was not observed near the Néel temperature. The only effect of an external magnetic field was to change the general attenuation level with field orientation. Fig. 6 shows that with the field parallel to the spin alignment direction (c axis) the attenuation was slightly increased.

The transition in  $\text{MnF}_2$  at  $\sim 67^\circ \text{K}$ . is thought to be<sup>17</sup> an order-disorder phase change between the two orientations of spins. A thermodynamic treatment of second order phase changes predicts that the thermal expansion coefficient, specific heat and isothermal compressibility of an isotropic solid should all become large at the transition temperature. From the measurements taken here it is apparent that any large changes in the compressibility must come about through changes in elastic constants other than those measured. Experiments to determine this effect, principally through changes in  $C_{33}$ , will be continued.

<sup>17</sup> T. Nagayama, K. Yosida and R. Kubo, *Ad Phys* **4**, 1 (1955)

# APPENDIX I

## CALCULATIONS

### 1. Velocity (based on $[110]$ direction of propagation)

#### (a) Velocity of longitudinally polarized waves, $[110]$ polarization.

$$V = \frac{2d}{t} \quad \begin{array}{l} d \text{ is thickness of sample, } 1.386 \text{ cm} \\ t \text{ is total transit time, } 4.2 \text{ microsec} \end{array}$$

$$V = \frac{2 \times 1.386 \text{ cm}}{4.20 \text{ microsec}} = 6.60 \times 10^5 \text{ cm sec}^{-1}$$

#### (b) Velocity of shear waves polarized parallel to c axis, $[001]$ polarization

$$\begin{array}{l} d \text{ remains } 1.386 \text{ cm} \\ t \text{ measured as } 9.45 \text{ microsec} \end{array}$$

$$V = \frac{2 \times 1.386 \text{ cm}}{9.45 \text{ microsec}} = 2.94 \times 10^5 \text{ cm sec}^{-1}$$

#### (c) Velocity of shear waves polarized perpendicular to c axis, $[110]$ polarization

$$\begin{array}{l} d \text{ remains } 1.386 \text{ cm} \\ t \text{ measured as } 17.10 \text{ microsec} \end{array}$$

$$V = \frac{2 \times 1.386 \text{ cm}}{17.10 \text{ microsec}} = 1.62 \times 10^5 \text{ cm sec}^{-1}$$

### 2. Attenuation

The slope of the calibrated exponential curve was in  $\text{sec}^{-1}$ . For attenuation in  $\text{db cm}^{-1}$  the following calculation was employed:

$$\text{Attenuation (in db cm}^{-1}\text{)} = \frac{\text{Slope of e curve (in sec}^{-1}\text{)} \times 8.636}{\text{Wave velocity (in cm sec}^{-1}\text{)}}$$

### 3. Elastic Constants, uncorrected for thermal expansion ( $[110]$ direction of propagation), $\rho = 3.891 \text{ gm cm}^{-3}$

#### (a) $[110]$ polarization

$$\rho C_{11} + \rho C_{12} + C_{66} = \rho V^2 = 3.891 \text{ gm cm}^{-3} \times (6.60 \times 10^5 \text{ cm sec}^{-1})^2$$

$$= 16.95 \times 10^{11} \text{ dyne cm}^{-2}$$

(b) [001] polarization

$$C_{44} = \rho v^2 = 3.891 \text{ gm cm}^{-3} \times (2.94 \times 10^5 \text{ cm sec}^{-1})^2 \\ = 3.363 \times 10^{11} \text{ dyne cm}^{-2}$$

(c) [110] polarization

$$\frac{1}{2}(C_{11} - C_{12}) = \rho v^2 = 3.891 \text{ gm cm}^{-3} \times (1.62 \times 10^5 \text{ cm sec}^{-1})^2 \\ = 1.021 \times 10^{11} \text{ dyne cm}^{-2}$$

#### 4. Correction for thermal expansion at 70° K.

$$L_{70} = L_{273} + \Delta L$$

$$\text{a axis: } \Delta L = 0.3 \times 10^{-4} \times L_{273} \\ L_{70} = L_{273} (1 + \epsilon_1)_{273}$$

$$\text{c axis: } \Delta L = -18.6 \times 10^{-4} \times L_{273} \\ L_{70} = L_{273} (1 + \epsilon_2)_{273}$$

$$\text{Vol}_{70} = L_a^2 L_c = L_{a273}^2 \times L_{c273} (1 + \epsilon_1)^2 (1 + \epsilon_2)$$

$$\rho_{70} = \frac{M}{\text{Vol}_{70}} = \frac{M}{V_{273} (1 + \epsilon_1)^2 (1 + \epsilon_2)}$$

$$v \text{ (velocity)} = \frac{L_a}{T} = L_{a273} \frac{(1 + \epsilon_1)}{T}$$

$$(\rho v^2)_{70} = \frac{M}{V_{273} (1 + \epsilon_1)^2 (1 + \epsilon_2)} \times \frac{(1 + \epsilon_1)^2}{T^2} L_{a273}^2 \\ = (\rho v^2)_{273} \times \frac{1}{1 + \epsilon_2}$$

$$= (\rho v^2)_{273} (1 - \epsilon_2)$$

$$= (\rho v^2)_{273} (1 - 18.6 \times 10^{-4})$$

$$(\rho v^2)_{70} = (\rho v^2)_{273} (0.9981)$$

This correction was applied to computations in part 3 of this appendix to provide data for Table 1.